Cryo–EM structure of the CRY2 and CIB1 fragment complex provides insights into CIB1-mediated photosignaling

Dear Editor,

Cryptochromes (CRYs) are blue-light photoreceptors that mediate various light responses in plants (Wang and Lin, 2020; Wang et al., 2021). Two CRYs have been identified in *Arabidopsis thaliana* (At), AtCRY1 and AtCRY2, which mediate hypocotyl elongation and floral initiation (Ahmad and Cashmore, 1993; Guo et al., 1998). CRYs are comprised of a conserved N-terminal photolyase-related (PHR) domain for chromophore FAD binding and a C-terminal domain (CCE) of variable length, and different plant CRYs have been found to exert overlapping biological functions (Lin et al., 1998; Rosenfeldt et al., 2008).

Upon illumination with blue light, AtCRY2 can directly modulate the transcription of *flowering locus T* through interaction with the N-terminal domain of CRY interaction basic-helix-loop-helix (bHLH) protein 1 (CIB1), a bHLH transcription factor (Liu et al., 2008). CIB1 is the first-identified downstream transcription factor that interacts with CRY2 in a blue light–dependent manner. It can form homodimers or heterodimers (with other CIBs) to bind with G/E-box DNA via bHLH, and G/E-box DNA is usually present in light-responsive gene promoters (Liu et al., 2013). Since the identification of CIB1, the AtCRY2–CIB1 complex has been engineered as an optical control switch and used extensively in optogenetics (Konermann et al., 2013; Wang and Lin, 2020). To elucidate the assembly and interaction mechanism of activated AtCRY2 and downstream CIB1, we determined the cryoelectron microscopy (cryo–EM) structures of a constitutively active AtCRY2 mutant and its complex with the CIB1 fragment.

To obtain an active sample for structural analysis, we generated the constitutively active AtCRY2 mutant AtCRY2^{W374A} (Li et al., 2011) and AtCIB1 truncates (Figure 1A), and we expressed them separately or together in insect cells. A two-step purification protocol (Shao et al., 2020), Ni^{2+}-chelating plus gel-filtration chromatography, was used to obtain a homogenous complex sample for cryo–EM analysis. It appeared that the CIB1 C-terminal truncates, CIB1^{NT275} (residues 1–275) and CIB1^{NT158} (residues 1–158), could form a complex with AtCRY2^{W374A}. Compared with AtCRY2^{W374A}, an obvious peak shift suggested formation of an AtCRY2^{W374A}–CIB1^{NT275} complex during gel-filtration purification (Figure 1B). The binding affinity between AtCRY2^{W374A} and CIB1^{NT275} was determined using bio-layer interferometry, yielding a dissociation constant of 3.90E−07 M, whereas no significant binding was detected between wild-type AtCRY2 and CIB1^{NT275} (Supplemental Figure 1). SDS–PAGE analysis indicated that AtCRY2^{W374A} and AtCIB1 proteins assemble in a 1:1 molar ratio. The resulting samples were used for cryo–EM

analysis after treatment with 2.0 mM bis(sulfosuccinimidyl) suberate.

The cryo–EM structure of AtCRY2^{W374A} was determined to an overall resolution of 2.56 Å, and a tetramer atomic model was built (Figure 1C and Supplemental Figures 2 and 3; Supplemental Table 1), which was much improved compared with previous reported structures (Ma et al., 2020a; Shao et al., 2020). However, because of the dynamic nature of the AtCRY2^{W374A}–CIB1 complex (Supplemental Video 1), numerous efforts were made to obtain an AtCRY2^{W374A}–CIB1 structure. The best density map of AtCRY2^{W374A}–CIB1^{NT275} was refined to 3.89 Å resolution (Figure 1D and 1E and Supplemental Figures 4 and 5; Supplemental Table 1), based on which the PHR domain of AtCRY2^{W374A} and partial secondary structural elements of CIB1 (Figure 1F) could be built (orange color). Additional density blobs (gray color) could be observed at the AtCRY2 Mol-BD (or AC) interface and were thought to be a CIB1 fragment, but the model could not be traced (Figure 1D and 1E). The CCEs in both structures were disordered. Nevertheless, the binding site of CRY2 to CIB1 could be clearly determined from the envelope structure.

Consistent with our previous study (Shao et al., 2020), two interaction surfaces were confirmed in the AtCRY2^{W374A} structure (Figure 1C): the conserved interaction surface 1 (INT1) formed by molecules AB (or CD) and the non-conserved INT2 formed by molecules AC (or BD). The CIB1 fragments bind at the INT2 regions in a side-by-side manner to the CRY2 tetramer in the AtCRY2^{W374A}–CIB1 complex structure (Figure 1D). We also noticed that the density of CIB1 molecules on the right side was clearer than that on the left side, probably owing to the dynamic nature of the complex (Supplemental Video 1). Two repeated secondary structural elements can be fairly deduced from the right-side CIB1 molecules (Figure 1D–1F), supporting a 1:1 molar ratio of AtCRY2 and CIB1.

Structural elements and residues of AtCRY2 involved in the CIB1 interaction can be defined from the current complex structure and include the α4 helix, β5–α5 loop, and L11 loop and the His113, Trp138, Tyr141, and Phe302 residues (Figure 1F). These residues were confirmed by mutation-based analysis, and pull-down results demonstrated that mutation of residue Trp138 or Tyr141 to Ala impaired the AtCRY2–CIB1 interaction, whereas mutation of His28 or Phe302 had less effect (Figure 1G). Supporting evidence also comes from a
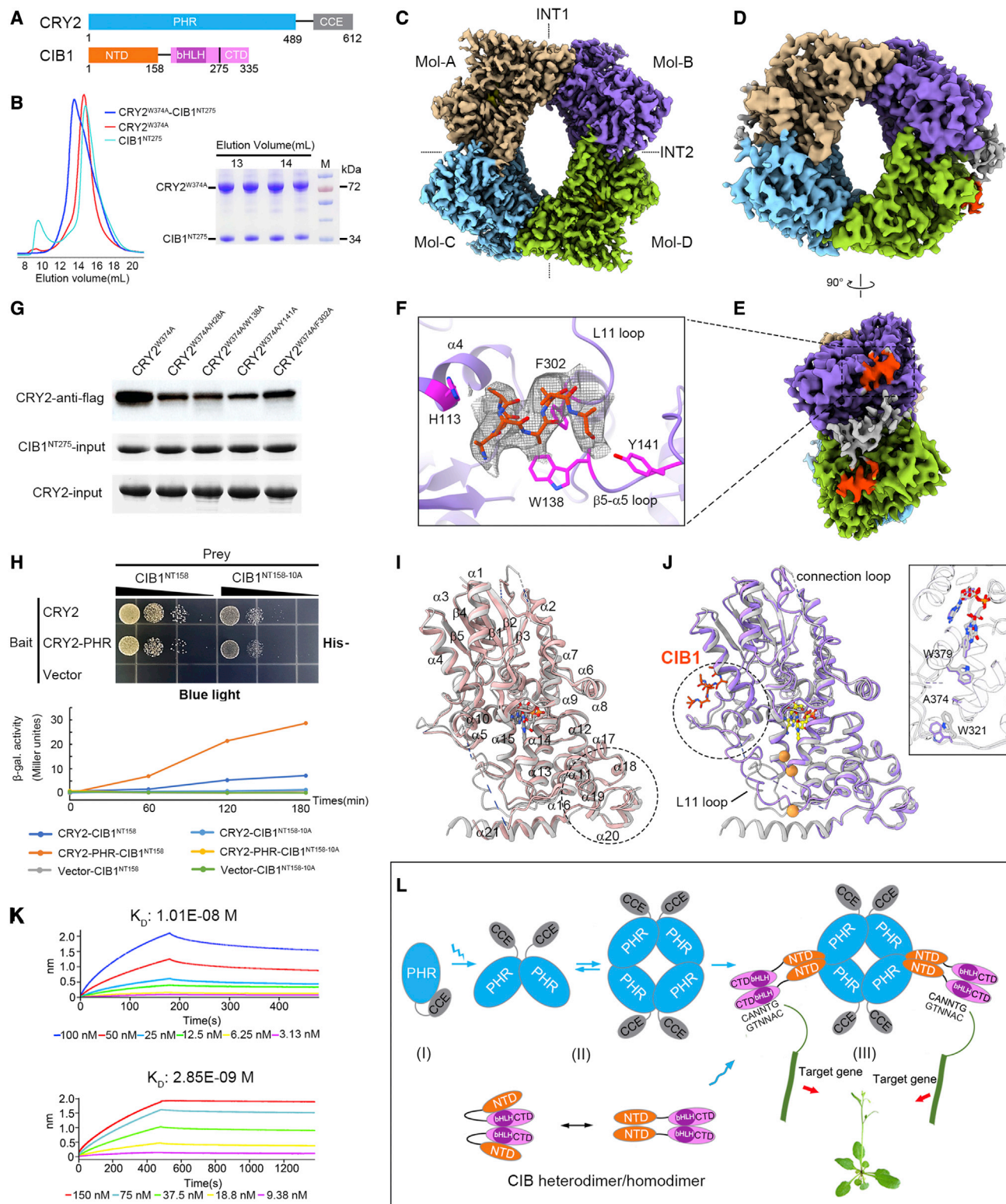
Figure 1. Cryo–EM structure of the CRY2–CIB1 complex.

(A) Color-coded domain architecture of CRY2 and CIB1 from *Arabidopsis thaliana*. CRY2 comprises a PHR domain and a non-conserved CCE domain. CIB1 contains an N-terminal domain (CIB1N) and a C-terminal domain (CIB1C). CIB1N is the CRY2-binding domain, whereas CIB1C, which contains the bHLH motif, interacts with DNA.

(B) SEC (size exclusion chromatography) profiles of the constitutively active mutant AtCRY2^{W374A} (red), the AtCRY2^{W374A}–CIB1^{NT275} complex (blue), and CIB1^{NT275} (cyan). Peak fractions of the AtCRY2^{W374A}–CIB1^{NT275} complex SEC were subjected to SDS–PAGE.

(legend continued on next page)

cross-linking mass spectrometry experiment in which lysine residues Lys116, Lys118, and Lys146 around INT2 were observed to interact with CIB1 as multi-crosslinked sites (Supplemental Figure 6; Supplemental Table 2).

Because it is difficult to trace the amino acids of CIB1 from the At-CRY2–CIB1 fragment complex structure, we used a yeast two-hybrid assay to map the interaction region of CIB1. Our previous data have demonstrated that residues 16–43 of CIB1 are essential for interaction with activated AtCRY2 (Shao et al., 2020) and that residues 18–27 tend to form an α-helix when predicted using AlphaFold (Jumper et al., 2021). We therefore generated a mutation within this region and found that mutation of 18–27 to Ala (CIB1$^{NT158–10A}$) significantly reduced the blue light–dependent interaction between CRY2 or CRY2–PHR and CIB1 (Figure 1H and Supplemental Figure 7), as demonstrated by reduced yeast growth and β-galactosidase activity. These results indicated that CIB1$^{18–27}$ plays a critical role in the CRY2–CIB1 interaction.

In the AtCRY2^{W374A} and AtCRY2^{W374A}–CIB1^{NT275} structures, each CRY monomer is comprised of α/β and α domains linked by the connection loop connecting helices α5–α6. We aligned these structures with the previously reported inactive AtCRY2N structure under darkness (PDB: 6K8I) (Ma et al., 2020b) and summarized the conformational changes within the monomers (with root-mean-square deviations around 1.4 Å using all pairs). In the activated AtCRY2^{W374A} structure, the relative movement of the α domain near INT1 (Figure 1I) and a fairly defined β5–α5 loop near INT2 (Supplemental Figure 8A and 8B) enable light-dependent formation of the CRY2 dimer and tetramer. The subsequent binding of CIB1 further induces more stabilized structures at the loops connecting α11–α12 (L11 loop) and α5–α6 (connection loop) (Figure 1J and Supplemental Figure 8A and 8C). In a zoomed-in view around the FAD molecule, the distal one of the "Trp triad" residues, Trp321, located in the L11 loop, undergoes a pronounced conformational change (Figure 1J, inset). Similar conformational changes of "Trp-triad" residues have been found during the photoactivation process of ZmCRY1c (Shao et al., 2020). This finding suggests that the CRY2 tetramer may adopt a more stable active conformation when binding with CIB1.

In the CRY2 tetramer, INT2 is formed by helices α2 and α10 and a connection loop from each molecule, and the interaction forces are mainly hydrophobic interactions. Binding of CIB1 to AtCRY2^{W374A} causes 15 (out of 85) more residues to be involved

in INT2 formation; at the same time, the buried surface area of INT2 increases by about 30% (from 1104 to 1627 Å^2 for Mol-BD, and from 1104 to 1504 Å^2 for Mol-AC) (Supplemental Figure 8D and 8E). By contrast, no obvious changes take place at the Mol-AB (or Mol-CD) dimer interface after CIB1 binding, as the buried surface area of INT1 shows little change (from 1494 to 1506 Å^2). A significant change is manifested by the shortened distance, from 7.1 to 3.7 Å, between the adjacent connection loops (Supplemental Figure 8F). In general, CIB1 binding induces an obvious relative movement of Mol-CD against Mol-AB (Supplemental Video 2), which can be simplified into a ~7° rotation and a 1.4 Å translation of Mol-CD along the y axis perpendicular to the INT2 plane (Supplemental Figure 9), resulting in a more compact AtCRY2 tetramer.

Because CIB1 can bind with G-box DNA (Liu et al., 2013), we tested the effect of the AtCRY2–CIB1 complex on the binding ability of CIB1 to DNA. Using the recombinantly expressed AtCRY2–CIB1 complex and synthesized G-box DNA, we found that the dissociation constant of CIB1 was about 1.01E−08 M, whereas that of the AtCRY2–CIB1^{NT275} complex was about 2.85E−09 M (Figure 1K), indicating that binding of AtCRY2 to CIB1 improves the binding affinity of the latter by about four-fold.

Based on structural analysis and biochemical experiments, we propose a possible working model of AtCRY2 photosignaling mediated by CIB proteins (Figure 1L). In the dark, inactive AtCRY2 exists mainly as a monomer. A small number of CIB homo- or hetero-dimers are in dynamic equilibrium, during which the DNA-binding ability of the C-terminal bHLH domain is relatively low. Upon blue-light illumination, AtCRY2 undergoes conformational changes and consequently forms an active oligomer (dimer and tetramer). Meanwhile, the expression of CIBs is upregulated (Liu et al., 2008). The N-terminal domain of CIB interacts with INT-2 of the active AtCRY2 homotetramer, not only strengthening AtCRY2 homotetramer formation but also enhancing the binding or association of CIBs with the target gene promoter, ultimately leading to transcriptional activation.

In summary, we present a representative three-dimensional structure of activated CRY binding with its downstream signaling protein CIB1. Structure-based analysis reveals that the blue light–induced oligomerization of AtCRY2 is required for downstream CIB1 binding, and the binding site of CIB1 on AtCRY2 is presented. Interestingly, binding of AtCRY2 with CIB1 further enhanced the DNA-binding ability of CIB1, and the mechanism underlying this effect requires further investigation. In addition,

---

(C) Cryo–EM map of the AtCRY2^{W374A} tetramer in front view contoured at 3 σ threshold. The four monomers labeled A, B, C, and D are colored wheat, purple, blue, and green, respectively. The INT1 and INT2 interfaces are indicated with dashed lines.

(D and E) Cryo–EM map of the AtCRY2^{W374A}–CIB1^{NT275} complex in front and side views contoured at 2.8 σ threshold. CIB1 fragments are colored orange, and the same color scheme of CRY2 is used in all figures. The additional CIB1 density blobs are colored gray.

(F) Zoomed-in view of CIB1 fragment binding with CRY2. Residues involved in interactions are labeled and shown as sticks. EM density of CIB1 fragment is contoured at 4σ threshold. **(G)** *In vitro* pull-down assay of CRY2^{W374A} mutants and CIB1^{NT275} complex.

(H) Growth phenotype of the yeast two-hybrid assay showing that CIB1$^{18–27}$ plays a critical role in the CRY2–CIB1 interaction. β-galactosidase activity was measured to quantify the results.

(I) Structure superimposition of CRY2 monomers from AtCRY2N (pink) and AtCRY2^{W374A} (gray) structures. α domain is indicated by a circle.

(J) Structure superimposition of CRY2 monomers from AtCRY2^{W374A} (gray) and AtCRY2^{W374A}–CIB1^{NT275} (purple) structures. CIB1 binding region is indicated by a circle. Trp-triad residues are shown as gold spheres. Inset, a close-up view of FAD and Trp-triad residues is shown.

(K) G-box binding affinity curves of CIB1^{NT275} (upper) and the AtCRY2^{W374A}–CIB1^{NT275} complex (lower). K$_D$, dissociation constant.

(L) A possible working model of AtCRY2 photosignaling mediated by CIB proteins. The blue zigzag represents blue light. I, CRY2 monomer in darkness; II, CRY2 dimer or tetramer upon blue-light illumination; III, active CRY2 tetramer forms a complex with CIB to mediate photosignaling.

because the CRY2–CIB light-inducible dimerization system has been used extensively for optogenetic applications, our study provides a structural basis for rational engineering of this light switch.

AUTHOR CONTRIBUTIONS
Y.H., X.Z., and P.Z. designed the experiments. Y.H. carried out the bulk of the experiments; X.Z. carried out cryo–EM data collection and structure determination; Y.L. and M.M. contributed to protein expression, purification, and BLI analysis; X.H. contributed to cryo–EM data collection; H.L. contributed to data analysis and discussion; and P.Z. wrote the manuscript with input from other authors.

Yahui Hao[1,2,3], Xue Zhang[1,3], Yaqi Liu[1,2],
Miaolian Ma[1], Xiaowei Huang[1,2], Hongtao Liu[1]
and Peng Zhang[1,*]

[1]National Key Laboratory of Plant Molecular Genetics, Center for Excellence in Molecular Plant Sciences, Institute of Plant Physiology and Ecology, Shanghai Institutes for Biological Sciences, Chinese Academy of Sciences, Shanghai, China
[2]University of Chinese Academy of Sciences, Beijing, China
[3]These authors contributed equally to this article.
*Correspondence: Peng Zhang (pengzhang01@cemps.ac.cn)
https://doi.org/10.1016/j.xplc.2022.100475

REFERENCES
Ahmad, M., and Cashmore, A.R. (1993). HY4 gene of A. thaliana encodes a protein with characteristics of a blue-light photoreceptor. Nature **366**:162–166.

Guo, H., Yang, H., Mockler, T.C., and Lin, C. (1998). Regulation of flowering time by Arabidopsis photoreceptors. Science **279**:1360–1363.

Jumper, J., Evans, R., Pritzel, A., Green, T., Figurnov, M., Ronneberger, O., Tunyasuvunakool, K., Bates, R., Žídek, A., Potapenko, A., et al. (2021). Highly accurate protein structure prediction with AlphaFold. Nature **596**:583–589.

Konermann, S., Brigham, M.D., Trevino, A., Hsu, P.D., Heidenreich, M., Cong, L., Platt, R.J., Scott, D.A., Church, G.M., and Zhang, F. (2013). Optical control of mammalian endogenous transcription and epigenetic states. Nature **500**:472–476.

Li, X., Wang, Q., Yu, X., Liu, H., Yang, H., Zhao, C., Liu, X., Tan, C., Klejnot, J., Zhong, D., and Lin, C. (2011). Arabidopsis cryptochrome 2 (CRY2) functions by the photoactivation mechanism distinct from the tryptophan (trp) triad-dependent photoreduction. Proc. Natl. Acad. Sci. USA **108**:20844–20849.

Lin, C., Yang, H., Guo, H., Mockler, T., Chen, J., and Cashmore, A.R. (1998). Enhancement of blue-light sensitivity of Arabidopsis seedlings by a blue light receptor cryptochrome 2. Proc. Natl. Acad. Sci. USA **95**:2686–2690.

Liu, H., Yu, X., Li, K., Klejnot, J., Yang, H., Lisiero, D., and Lin, C. (2008). Photoexcited CRY2 interacts with CIB1 to regulate transcription and floral initiation in Arabidopsis. Science **322**:1535–1539.

Liu, Y., Li, X., Li, K., Liu, H., and Lin, C. (2013). Multiple bHLH proteins form heterodimers to mediate CRY2-dependent regulation of flowering-time in Arabidopsis. PLoS Genet. **9**:e1003861.

Ma, L., Guan, Z., Wang, Q., Yan, X., Wang, J., Wang, Z., Cao, J., Zhang, D., Gong, X., and Yin, P. (2020a). Structural insights into the photoactivation of Arabidopsis CRY2. Nat. Plants **6**:1432–1438.

Ma, L., Wang, X., Guan, Z., Wang, L., Wang, Y., Zheng, L., Gong, Z., Shen, C., Wang, J., Zhang, D., et al. (2020b). Structural insights into BIC-mediated inactivation of Arabidopsis cryptochrome 2. Nat. Struct. Mol. Biol. **27**:472–479.

Rosenfeldt, G., Viana, R.M., Mootz, H.D., von Arnim, A.G., and Batschauer, A. (2008). Chemically induced and light-independent cryptochrome photoreceptor activation. Mol. Plant **1**:4–14.

Shao, K., Zhang, X., Li, X., Hao, Y., Huang, X., Ma, M., Zhang, M., Yu, F., Liu, H., and Zhang, P. (2020). The oligomeric structures of plant cryptochromes. Nat. Struct. Mol. Biol. **27**:480–488.

Wang, Q., and Lin, C. (2020). Mechanisms of cryptochrome-mediated Photoresponses in plants. Annu. Rev. Plant Biol. **71**:103–129.

Wang, W., Mao, Z., Guo, T., Kou, S., and Yang, H.-Q. (2021). The involvement of the N-terminal PHR domain of Arabidopsis cryptochromes in mediating light signaling. aBIOTECH **2**:146–155.